Near-field probing of Mie resonances in single TiO2 microspheres at terahertz frequencies

Oleg Mitrofanov, Filip Dominec, Petr Kužel, John L. Reno, Igal Brener, U-Chan Chung, Catherine Elissalde, Mario Maglione, Patrick Mounaix

Near-field probing of Mie resonances in single TiO₂ microspheres at terahertz frequencies

Oleg Mitrofanov,[1,2,*] Filip Dominec,[3] Petr Kužel,[3] John L. Reno,[2,4] Igal Brener,[2,4] U-Chan Chung,[5] Cathy Elissalde,[5] Mario Maglione,[5] and Patrick Mounaix[6]

[1]*University College London, London, WC1E 7JE, UK*
[2]*Center for Integrated Nanotechnologies, Sandia National Laboratories, Albuquerque, NM 87185, USA*
[3]*Academy of Sciences of the Czech Republic, 182 21 Prague, Czech Republic*
[4] *Sandia National Laboratories, Albuquerque, NM 87185, USA*
[5]*ICMCB, Univ. Bordeaux, CNRS, UPR 9048, 33600 Pessac cedex, France*
[6]*LOMA, Univ. Bordeaux, CNRS, UMR 5798, 33405 Talence, France*
[*]*o.mitrofanov@ucl.ac.uk*

Abstract: We show experimentally that poly-crystalline TiO₂ spheres, 20-30 μm in diameter, exhibit a magnetic dipole Mie resonance in the terahertz (THz) frequency band (1.0-1.6 THz) with a narrow line-width (<40 GHz). We detect and investigate the magnetic dipole and electric dipole resonances in single high-permittivity TiO₂ microspheres, using a near-field probe with a sub-wavelength (~λ/50) size aperture and THz time-domain spectroscopy technique. The Mie resonance signatures are observed in the electric field amplitude and phase spectra, as well as in the electric field distribution near the microspheres. The narrow line-width and the sub-wavelength size (λ/10) make the TiO₂ microspheres excellent candidates for realizing low-loss THz metamaterials.

References and links

1. D. Schurig, J. J. Mock, B. J. Justice, S. A. Cummer, J. B. Pendry, A. F. Starr, and D. R. Smith, "Metamaterial electromagnetic cloak at microwave frequencies," Science **314**(5801), 977–980 (2006).
2. D. R. Smith, J. B. Pendry, and M. C. K. Wiltshire, "Metamaterials and negative refractive index," Science **305**(5685), 788–792 (2004).
3. H. Tao, W. J. Padilla, X. Zhang, and R. D. Averitt, "Recent progress in electromagnetic metamaterial devices for terahertz applications," IEEE J. Sel. Top. Quantum Electron. **17**(1), 92–101 (2011).
4. R. Merlin, "Metamaterials and the Landau-Lifshitz permeability argument: Large permittivity begets high-frequency magnetism," Proc. Natl. Acad. Sci. U.S.A. **106**(6), 1693–1698 (2009).
5. A. I. Kuznetsov, A. E. Miroshnichenko, Y. H. Fu, J. Zhang, and B. Luk'yanchuk, "Magnetic light," Sci. Rep. **2**, 492 (2012).
6. J. M. Geffrin, B. Garcıa-Etxarri, R. Gómez-Medina, P. Albella, L. S. Froufe-Pérez, C. Eyraud, A. Litman, R. Vaillon, F. González, M. Nieto-Vesperinas, J. J. Sáenz, and F. Moreno, "Magnetic and electric coherence in forward- and back-scattered electromagnetic waves by a single dielectric subwavelength sphere," Nat. Commun. **3**, 1171 (2012).
7. L. Lewin, "The electrical constants of a material loaded with spherical particles," J. Inst. Electr. Eng. Part III **94**(27), 65–68 (1947).
8. S. O'Brien and J. B. Pendry, "Photonic band-gap effects and magnetic activity in dielectric composites," J. Phys. Condens. Matter **14**(15), 4035–4044 (2002).
9. B.-I. Popa and S. A. Cummer, "Compact dielectric particles as a building block for low-loss magnetic metamaterials," Phys. Rev. Lett. **100**(20), 207401 (2008).
10. Q. Zhao, L. Kang, B. Du, H. Zhao, Q. Xie, X. Huang, B. Li, J. Zhou, and L. Li, "Experimental demonstration of isotropic negative permeability in a three-dimensional dielectric composite," Phys. Rev. Lett. **101**(2), 027402 (2008).
11. Q. Zhao, J. Zhou, F. Zhang, and D. Lippens, "Mie resonance-based dielectric metamaterials," Mater. Today **12**(12), 60–69 (2009).
12. K. Vynck, D. Felbacq, E. Centeno, A. I. Căbuz, D. Cassagne, and B. Guizal, "All-dielectric rod-type metamaterials at optical frequencies," Phys. Rev. Lett. **102**(13), 133901 (2009).
13. J. C. Ginn, I. Brener, D. W. Peters, J. R. Wendt, J. O. Stevens, P. F. Hines, L. I. Basilio, L. K. Warne, J. F. Ihlefeld, P. G. Clem, and M. B. Sinclair, "Realizing optical magnetism from dielectric metamaterials," Phys. Rev. Lett. **108**(9), 097402 (2012).

14. H. Němec, P. Kužel, F. Kadlec, C. Kadlec, R. Yahiaoui, and P. Mounaix, "Tunable terahertz metamaterials with negative permeability," Phys. Rev. B **79**(24), 241108 (2009).
15. K. Shibuya, K. Takano, N. Matsumoto, K. Izumi, H. Miyazaki, Y. Jimba, and M. Hangyo, "Terahertz metamaterials composed of TiO₂ cube arrays," in *Proceedings of Congress on Advanced Electromagnetic Mater. in Microw. and Opt.* (2008), pp. 777–779.
16. H. Němec, C. Kadlec, F. Kadlec, P. Kužel, R. Yahiaoui, U.-C. Chung, C. Elissalde, M. Maglione, and P. Mounaix, "Resonant magnetic response of TiO₂ microspheres at terahertz frequencies," Appl. Phys. Lett. **100**(6), 061117 (2012).
17. M. Navarro-Cía, M. Natrella, F. Dominec, J. C. Delagnes, P. Kuzel, P. Mounaix, C. Graham, C. C. Renaud, A. J. Seeds, and O. Mitrofanov, "Terahertz imaging of sub-wavelength particles with Zenneck surface," Appl. Phys. Lett. **103**(22), 221103 (2013).
18. O. Mitrofanov, M. Lee, J. W. P. Hsu, I. Brener, R. Harel, J. Federici, J. D. Wynn, L. N. Pfeiffer, and K. W. West, "Collection mode near-field imaging with 0.5 THz pulses," IEEE J. Sel. Top. Quantum Electron. **7**(4), 600–607 (2001).
19. J. R. Knab, A. J. L. Adam, E. Shaner, H. J. A. J. Starmans, and P. C. M. Planken, "Terahertz near-field spectroscopy of filled subwavelength sized apertures in thin metal films," Opt. Express **21**(1), 1101–1112 (2013).
20. O. Mitrofanov, W. Yu, R. J. Thompson, Y. Jiang, I. Brener, W. Pan, C. Berger, W. A. De Heer, and Z. Jiang, "Probing terahertz surface plasmon waves in graphene structures," Appl. Phys. Lett. **103**(11), 111105 (2013).
21. K. Aydin, A. O. Cakmak, L. Sahin, Z. Li, F. Bilotti, L. Vegni, and E. Ozbay, "Split-ring-resonator-coupled enhanced transmission through a single subwavelength aperture," Phys. Rev. Lett. **102**(1), 013904 (2009).
22. V. Sadaune, L. Kang, and D. Lippens, "Enhanced transmission via a sub-wavelength hole aperture coupled to a high-permittivity resonator," J. Phys. D Appl. Phys. **45**(47), 475102 (2012).
23. A. J. Macfaden, J. L. Reno, I. Brener, and O. Mitrofanov, "3 μm aperture probes for near-field terahertz transmission microscopy," Appl. Phys. Lett. **104**(1), 011110 (2014).
24. L. Kang, V. Sadaune, and D. Lippens, "Numerical analysis of enhanced transmission through a single subwavelength aperture based on Mie resonance single particle," Prog. Electromagn. Res. **113**, 211–226 (2011).
25. B. Luk'yanchuk, N. I. Zheludev, S. A. Maier, N. J. Halas, P. Nordlander, H. Giessen, and C. T. Chong, "The Fano resonance in plasmonic nanostructures and metamaterials," Nat. Mater. **9**(9), 707–715 (2010).
26. A. F. Oskooi, D. Roundy, M. Ibanescu, P. Bermel, J. D. Joannopoulos, and S. G. Johnson, "MEEP: A flexible free-software package for electromagnetic simulations by the FDTD method," Comput. Phys. Commun. **181**(3), 687–702 (2010).
27. See http://www.lumerical.com/tcad-products/fdtd/ for Lumerical FDTD Solutions, Lumerical Solutions, Inc.
28. D. L. Markovich, P. Ginzburg, A. K. Samusev, P. A. Belov, and A. V. Zayats, "Magnetic dipole radiation tailored by substrates: numerical investigation," Opt. Express **22**(9), 10693–10702 (2014).
29. R. Singh, I. A. I. Al-Naib, M. Koch, and W. Zhang, "Sharp Fano resonances in THz metamaterials," Opt. Express **19**(7), 6312–6319 (2011).

1. Introduction

The concept of metamaterials has enabled design of electromagnetic functionalities, which do not occur in natural materials. This has led to the realization of intriguing electromagnetic phenomena, such as cloaking [1] and negative refraction [2]. One of the key elements for metamaterials is a sub-wavelength size resonator with an effective magnetic response. Metallic split-ring resonators (SRR) are often used for that purpose [3]. However, the SSRs show a less than ideal behavior due to their anisotropy, polarization dependent response and spectral broadening caused by metallic Ohmic losses. For these reasons, arrays of dielectric resonators have attracted much interest recently. A magnetic response can be produced in a high-permittivity, sub-wavelength size dielectric particle as a result of the lowest order resonance, known as the 1st Mie mode or the magnetic dipole (MD) mode [4–6]. An array of such resonators exhibits a macroscopic magnetic response with negative values of permeability μ in the wavelength range determined by the resonator size [7–15]. Similarly, a negative dielectric response $\varepsilon<0$ can be realized using the second Mie mode, known as the electric dipole (ED) mode [5–13, 15].

High-permittivity materials ($\varepsilon>20$) are rare in the optical part of the electromagnetic (EM) spectrum. At terahertz (THz) frequencies however, some materials, for example rutile compounds, exhibit $\varepsilon>100$ and moderate losses [15]. The MD resonance in the region of 1 THz is expected for a microsphere, 30 μm in diameter, made of TiO₂ ($\varepsilon\approx100$). An ensemble of such TiO₂ microspheres was recently shown to exhibit a resonant spectral signature due to the MD Mie mode at 0.7-0.9 THz [16]. The inhomogeneous line-width broadening of 0.2 THz however obscured the intrinsic resonator properties. The resonance frequency of each

microsphere depends sensitively on the resonator size and shape, as well as the crystallinity and porosity of TiO_2, all of which varied within the ensemble [16].

In order to determine the intrinsic line-widths of the MD and ED modes, the TiO_2 microspheres should be probed individually. We estimate that a single TiO_2 sphere of radius r = $\lambda/(2n)$ = $\lambda/20$ (assuming $\varepsilon = n^2 = 100$) placed in the focus of a typical THz beam produces small attenuation (~1%) of the beam intensity at the frequency of MD resonance. This small value of attenuation is due to the reduction of the scattering cross-section at the MD resonance for high-permittivity resonators. In the vicinity of a high-permittivity resonator, on the other hand, the electromagnetic energy of the incident wave is concentrated. Near-field microscopy methods therefore may provide an alternative method for probing the resonator modes. Concentration of THz surface (Zenneck) waves near high-permittivity sub-wavelength size particles, including a TiO_2 microsphere, was recently observed with THz near-field microscopy [17]. Spectroscopic signatures of the Mie modes however were not detected [17].

Here, we investigate the MD and ED modes in single TiO_2 resonators using THz near-field microscopy in the transmission configuration [18–20]. We exploit the effect of the resonator on transmission of a plane wave through a sub-wavelength size aperture [21,22]. We observe clear signatures for the MD and ED modes by applying THz time-domain spectroscopy analysis. The MD mode displays a narrow resonance, several times narrower than the line-width observed in the far-field ensemble study [16].

2. Results and discussion

2.1 Experimental

For our studies, poly-crystalline TiO_2 microspheres are prepared by assembling and annealing clusters of TiO_2 nano-crystals [15]. The nano-crystals were mixed with ethanol to obtain a liquid suspension, which was then dried by spraying it through a flame. In this process the nano-crystals assemble into nearly spherical clusters, which solidify after annealing at 1200° C for 2 hours. The annealing time and temperature affect the packing density of nano-crystals in the clusters. Scanning electron micrographs show that the nano-crystals within the clusters are densely packed [Fig. 1(a)]. There are small voids between randomly oriented nano-crystals. Due to the sub-wavelength size of the nano-crystals and voids, and their random orientation, the dielectric function can be assumed to be isotropic. After comparing the size of similar microspheres to their resonance wavelength, we estimate the relative dielectric constant to be in the region of 90-100 [16].

Microsphere samples ranging in diameter between 20 and 30 μm were picked from the batch randomly and mounted on a 12.5 μm thick low-dielectric constant polymer film (polyvinyl chloride) with a thin layer of adhesive (cyanoacrylate). The thin-film substrate is chosen to reduce its effect on the resonator properties. The microsphere position is controlled by an automated XYZ translation stage.

The sample is illuminated by a ~0.5 mm diameter beam of single-cycle THz pulses (0.5-2.5 THz) generated by the process of optical rectification in a ZnTe crystal. A sub-wavelength size aperture in a 300 nm Au film on GaAs is positioned below the sphere as illustrated schematically in Fig. 1(b) [23]. The aperture size of 5 μm or 10 μm is chosen to be several times smaller than the microsphere diameter and substantially smaller than the wavelength (120-600 μm). A photo-conductive THz antenna is integrated into the system in the near-field zone of the aperture [Fig. 1(b)], ~1 μm below the aperture plane [23]. The antenna is oriented along the polarization direction of the incident THz beam (x-axis).

2.2 THz near-field spectroscopy and imaging of TiO_2 spheres

The effect of the sphere on the THz beam transmission through the aperture can be understood as the localization of the resonant field near the sphere due to (1) the reduced effective wavelength and (2) energy trapping inside the resonator. The localized field couples through the sub-wavelength aperture more efficiently than the incident THz beam, resulting

3

in enhanced transmission at the frequency of the Mie resonance. Recent numerical studies showed that the power transmission through a $\lambda/20$ aperture can be enhanced by up to 50 times when the dielectric resonator is positioned in front of the aperture [24]. This effect was utilized to probe a dielectric cube resonator at microwave frequencies [22].

The transmission enhancement effect is observed in the electric field map $E_x(x,y)$ measured by scanning a spherical TiO$_2$ particle ~27 μm in diameter (Sample T1) with respect to the aperture in the xy-plane at a distance $z \approx 1$ μm [Fig. 1(c)]. The image displays an enhanced electric field (negative value) in the region of the sphere at a moment immediately after the excitation by the THz pulse ($t = 1.33$ ps).
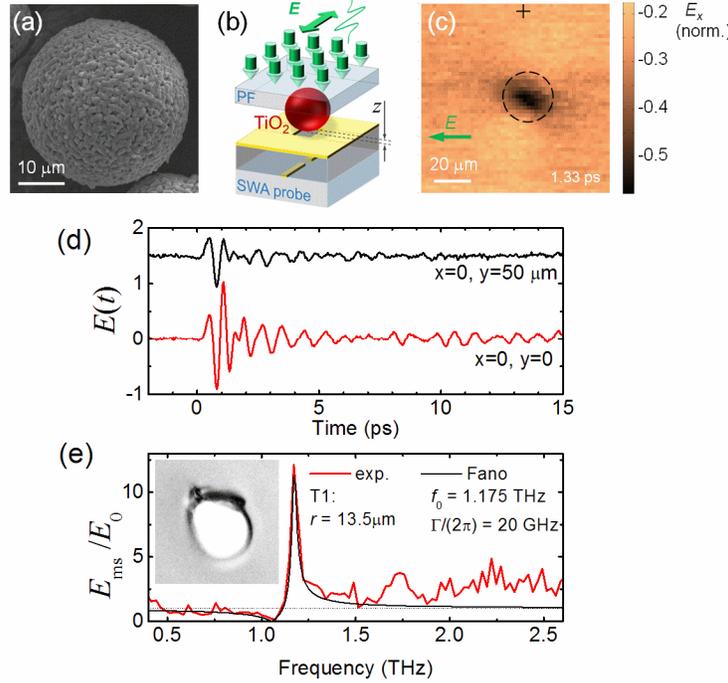

Fig. 1. (a) Scanning electron microscope image of a typical poly-crystalline TiO$_2$ sphere; (b) Schematic diagram of the experimental setup: a TiO$_2$ sphere attached to a thin polymer film (PF) is positioned at distance z above the sub-wavelength aperture (SWA) probe containing a photoconductive THz antenna [23]. (c) A map of the electric field (E_x) near a TiO$_2$ sphere immediately after the excitation (Sample T1). The dashed circle shows the sphere size and position. The black cross marks a location where the incident THz pulse waveform is measured for reference. (d) THz pulse waveforms detected in the near-field zone of the sphere (red trace) and at the cross location (black trace). (e) The amplitude transmission spectrum (red line) obtained from the waveforms in (d) and the Fano line shape (black line) fitted to the data; *inset:* an optical microscope image (60 μm × 60 μm) of Sample T1.

The region of enhanced field has an oblong shape with the long axis aligned to the incident field polarization direction (x-axis). The oblong shape reflects the electric field distribution near the resonator rather than the resonator's slightly elongated shape. It will be shown later using numerical simulations that an ideal sphere produces a similar oblong field pattern. We note that the aperture size is several times smaller than the size of the enhanced field region and therefore the aperture shape (5 μm x 5 μm square) is not reflected in the observed images. The THz image shows weaker lobes above and below the sphere, corresponding to the x-component of the field switching its sign outside the sphere.

Analysis of the THz pulse time-domain waveforms reveals that the enhanced transmission through the aperture occurs only at selected frequencies. The waveform measured by the 5 μm aperture probe when the microsphere is directly above the aperture [Fig. 1(d), red trace] displays coherent regular oscillations lasting over several cycles. The oscillations are absent

in the waveform of the incident reference pulse [Fig. 1(d), black trace], measured ~50 μm away from the sphere, at a location marked by the black cross, where the effect of the sphere is negligible. The oscillations indicate that a resonance is formed inside the sphere.

The ratio of the Fourier transform spectra E_{ms}/E_0 shows that the transmission amplitude decreases close to 0 at 1.1 THz and then rises to the level of ~12 (~150 in intensity) at a slightly higher frequency (1.175 THz). The observed transmission amplitude signature, similar to recent microwave scattering parameter measurements on a high-permittivity resonator [22], follows a Fano line shape [25]:

$$\frac{E_{ms}}{E_0} = \sqrt{\frac{\left(\frac{q\Gamma}{2} + (\omega - \omega_0)\right)^2}{(\Gamma/2)^2 + (\omega - \omega_0)^2}}, \tag{1}$$

where the Mie resonance frequency $\omega_0/2\pi = 1.175$ THz and the resonance line-width parameter $\Gamma/(2\pi) = 0.02 \pm 0.01$ THz [Fig. 1(e)]. q is the Fano parameter. It quantifies the aperture transmission enhancement factor at the resonance frequency: $E_{ms}/E_0 = q$.

The resonance line-width for the observed asymmetric line shape can be estimated by fitting the Fano line shape to the data. The Fano shape (Eq. (1)) changes to the Lorentzian shape for $q = 0$. The MD resonance full width at half maximum, which would be measured in a far-field transmission measurement, therefore is expected to be equal to $\Gamma/(2\pi) = 20 \pm 10$ GHz. We note however that the fitted line-width is similar to the measurement resolution line-width of 40 GHz, which we estimate from the duration of the recorded waveform (25 ps). Therefore we can conclude only that the observed line-width for Sample T1 is less than 40 GHz.

The spectrum also shows a smaller peak at ~1.7 THz. The set of two resonances matches the lowest order Mie modes, the MD and ED modes [Figs. 2(a) and 2(b)], simulated for a spherical particle with $\varepsilon \approx 100$. The simulations presented in Fig. 2 are performed with the finite-difference time-domain method (FDTD) using a freely available software package [26]. Similar spectra with the first resonance frequency ranging from 1.1 to 1.6 THz and the second frequency ranging from 1.6 to 2.0 THz are measured for five nearly spherical TiO_2 particles, ranging in size from 20 μm to 30 μm. The ratio of the sphere radius to the MD resonance wavelength $r/\lambda \approx 0.05$ is consistent with the assumption that the average dielectric function $\varepsilon \approx 100$.

The observed resonances confirm that the enhanced coupling effect is due to the excitation of normal modes in the microsphere (TiO_2 has no material-related modes in this spectral range). The resonance frequencies decrease as the resonator size increases, whereas their ratio $\omega_{MD}/\omega_{ED} \approx 0.7$ varies slightly from sample to sample. We attribute this variation to the non-ideal shape of the samples. Figures 2(c) and 2(d) illustrate the dependence of the resonance frequencies for an ellipsoid with semi-axes a, b and c.

The EM simulations in Figs. 2(a) and 2(b) also show that the modes are confined within the sphere, with only a small fraction of the mode energy leaking outside. To detect this confined field, the near-field probe must be positioned within a short distance from the sphere. The mode confinement is illustrated in the map of the transmission spectra (Sample T2) measured for z ranging from 0 to 40 μm [Fig. 3(a)]. As the microsphere is moved away from the aperture, the detected signatures of the MD resonance at 1.4 THz and the ED resonance at 2.0 THz decrease in amplitude. By fitting the Fano function to the experimental data [Fig. 3(b)], we find that the enhancement factor for the MD mode, q, decreases rapidly within short distance from the sphere, $0 < z < 15$ μm [Fig. 3(a)].
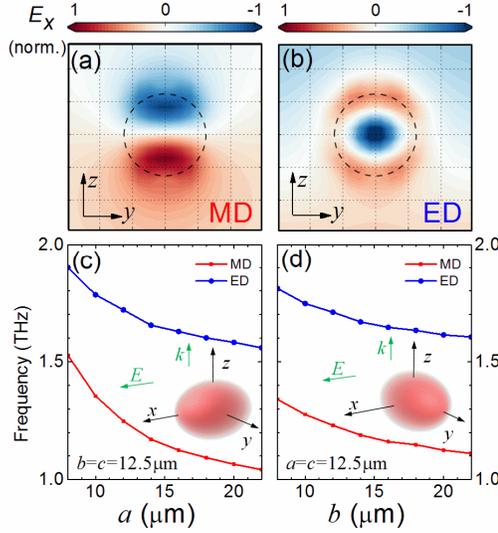
Fig. 2. (a) FDTD simulated MD (1.21 THz) and (b) ED (1.66 THz) modes in a TiO$_2$ sphere (ε = 100, radius r = 12.5 μm); the x-polarized incident EM wave propagates along the z-axis. The color represents the electric field (E_x) normalized to the maximum field within the sphere. (c) and (d) Resonance frequencies of the MD and ED modes in an elliptical resonator.

Fitting a Fano line shape to the data in Fig. 3 allows us to quantify the effect of the probe on the resonator characteristics. The line-width parameter for the MD mode remains constant within the experimental error: $\Gamma/(2\pi) = 0.05 \pm 0.01$ THz. The resonance frequency however shifts slightly from $f_0 = 1.43$ THz for the case of $z = 0$ μm to 1.37 THz for $z > 15$ μm. Accuracy of the extracted parameters for the MD resonance is however limited due to the measurement resolution and deviation of the experimental line shape from the ideal Fano line shape.

To verify the observed trends, we simulate the electromagnetic field distribution for an ideal sphere ($\varepsilon = 100$, $r = 12.5$ μm) placed in close proximity to a metallic plane with a 5 μm aperture. The simulations are performed with the FDTD method using a commercially available software package [27]. The electric field distribution in the xz-plane intersecting the sphere at its center is shown in Fig. 3(c) for two separations between the plane and the sphere: $z = 1$ μm (left) and $z = 4$ μm (right). The displayed field amplitude $|E|$ is normalized to its maximum value inside the sphere. For the separation of 1 μm, the metallic plane noticeably perturbs the field distribution outside the sphere. Inside the sphere however, the effect of the metallic plane is weak: only small asymmetry appears in the azimuthally symmetric field distribution of the MD mode. For the separation of 4 μm, the field inside the resonator exhibits practically no asymmetry due to the metallic plane. The near-field probe therefore preserves the MD resonance in TiO$_2$ microspheres.
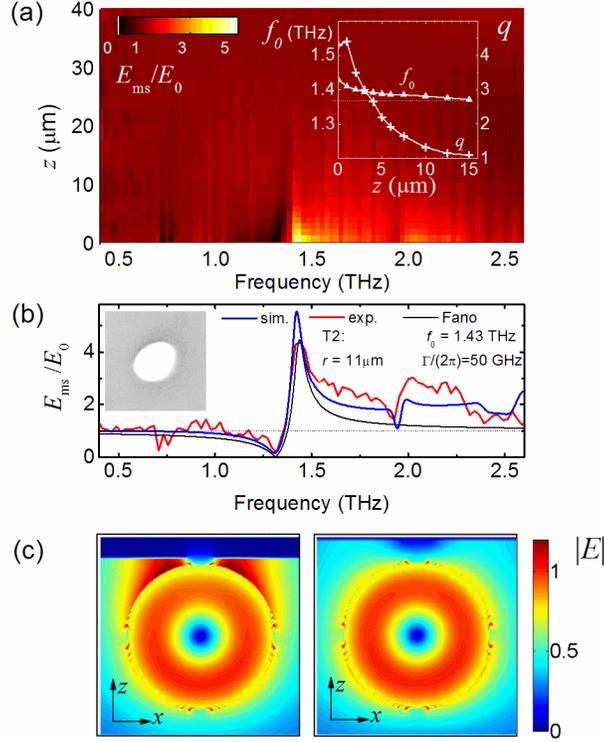
Fig. 3. (a) Dependence of the transmission amplitude spectrum E_{ms}/E_0 on the distance z between the aperture and the microsphere (Sample T2); inset: the resonance frequency f_0 and the enhancement factor q as functions of z. (b) The amplitude spectrum for the closest distance $z < 1$ μm measured by a 5 μm aperture probe (red line), the fitted Fano resonance line shape (black line) and the simulated spectrum of a TiO_2 sphere; *inset:* the optical microscope image (60 μm × 60 μm) of Sample T2. (c) The simulated field distributions for a sphere ($r = 12.5$ μm) placed in front of the near-field probe at the MD resonance; the metallic screen with a 5 μm aperture is 1 μm (left) and 4 μm (right) away from the sphere surface.

The simulated transmission spectra for the aperture with and without the sphere allow us to compare the numerical modeling with the experimentally recorded spectra. The normalized amplitude spectra E_{ms}/E_0 display remarkable similarities with the experiment. In Fig. 3(b), we illustrate the agreement between the experiment and simulations for a sphere of radius $r = 11$ μm and $\varepsilon = 94.2 + 1.16i$. The line shapes and the resonance frequencies for the MD and ED modes are in close agreement with the measured spectrum. The transmission enhancement factor at the MD resonance is slightly higher for the simulated spectrum. The enhancement factor however depends sensitively on the distance between the sphere and the aperture, as shown in the inset of Fig. 3(a).

The effect of the metallic screen on the MD resonance characteristics (frequency and line-width) is small for TiO_2 resonators. The resonance frequency shift due to the metallic probe is only 0.3% in the simulations. It is attributed to the strong mode localization by the high-permittivity material. We note that the shift increases for smaller permittivity resonators. It was recently reported that the MD resonance frequency shifts by ~0.6% for a $\varepsilon = 20$ sphere resting on a metallic plane in comparison with the sphere in free space [28]. The dielectric substrate can affect the resonance properties as well [28], however the low-permittivity and the sub-wavelength thickness of the substrate used in our experiments produce no noticeable effect. This is verified by comparing spectra measured for one sphere placed directly on the aperture screen with and without the polymer film substrate [Fig. 1(b)].

2.3 Effects of resonator non-sphericity

The MD mode in Sample T2 has a broader line-width than that in Sample T1 by a factor of 2 and it displays a 'shoulder' on the high-frequency side of the resonance. We attribute this line-width broadening to the resonator shape. All samples in this study deviate slightly from a perfect sphere [Figs. 1(e) and 3(b)]. While the MD resonance in an ideal sphere is 3-fold degenerate, the degeneracy is lifted in an ellipsoid. Three orthogonal MD modes can be excited if the incident wave polarization is not aligned with any of the ellipsoid principal axes. The spectral response of the resonator in this case is a superposition of projections of these modes on the detector antenna axis. The observed MD line-width therefore can be broadened by the resonator non-sphericity.

To verify the presence of MD modes with different orientations we use spatial mapping in the xy-plane at various moments after the THz pulse excitation. Panel (a) in Fig. 4 shows a THz image of a TiO$_2$ resonator (Sample T3) at the moment immediately after the THz pulse arrival. The field profile has an oblong shape, as the profile in Fig. 1(c). A similar shape is predicted by the FDTD simulations for an ideal sphere, as shown in the electric field map in Fig. 4(b), simulated for a moment immediately after the short pulse excitation.

Approximately 5 ps after the incident pulse, the experimental E_x map displays a very different pattern, anti-symmetric with respect to the y-axis [Fig. 4(c)]. A mode of this symmetry can be excited by the incident THz pulse only in the case of a non-spherical resonator. Such a pattern does not appear in the simulations of an ideal spherical resonator.
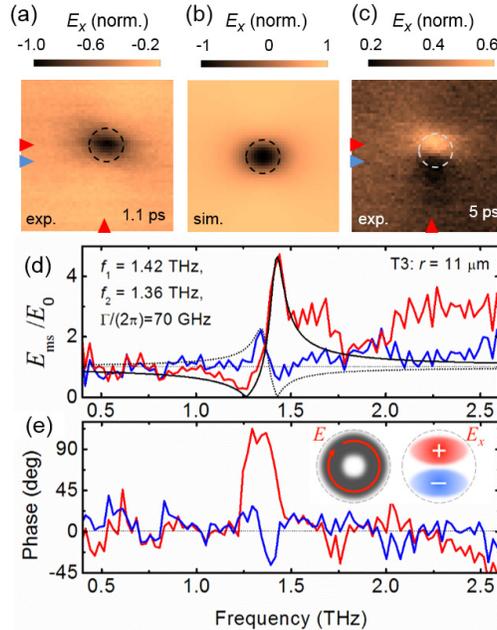

Fig. 4. Measured (a) and simulated (b) electric field maps $E_x(x,y)$ at $z = {\sim}1$ μm from the TiO$_2$ sphere immediately after the excitation of the sphere by the THz pulse, $t = 1.1$ ps (image area: 100 μm × 100 μm). (c) $E_x(x,y)$ map of the same area at $t = 5$ ps. The spectral amplitude ratio (d) and phase (e) measured at the sphere center (x_0, y_0) and at $(x_0, y_0-10$ μm); these location are indicated by the red and blue arrows in (a) and (c). The diagram in the inset of (e) shows the electric field distributions $|E|$ and E_x for the MD mode with the magnetic moment perpendicular to the xy-plane.

The origin of the pattern in Fig. 4(c) is determined by analyzing the detected THz spectra at two locations marked by the red and blue arrows in the images: at the resonator center (x_0,y_0); and at the anti-symmetric mode maximum $(x_0, y_0-10$ μm). In both cases, the spectra show resonances in the frequency region of the MD mode (~1.4 THz), however the line-shape

for the anti-symmetric mode is reversed [Fig. 4(d)]. The change of the line shape correlates with the phase spectra shown in [Fig. 4(e)]. The spectral signatures confirm the presence of two modes.

The resonance frequency of the anti-symmetric mode (f_2 = 1.36 THz) is slightly different from that of the symmetric mode (f_1 = 1.42 THz), indicating that the MD mode degeneracy is lifted. While the strong resonance at f_1 corresponds to the MD mode with a large projection of its magnetic moment on the y-axis, the weaker resonance at f_2 correspond to a MD mode with a different orientation. The dipole moment for f_2 must have a non-zero projection on the z-axis, as the observed anti-symmetric field profile in Fig. 4(c) matches the corresponding E_x distribution [inset of Fig. 4(e)].

The small difference in their resonance frequencies allows us to detect the presence of the two MD resonances with different orientations of their magnetic dipole moments in the temporally resolved field distribution. After the THz pulse excitation, the relative phase between the coherent oscillations of the two dipole moments increases over time. For f_1–f_2 = 60 GHz, a $\pi/2$ phase shift is accumulated ~4-5ps after the excitation. Around that moment in time, the oscillating field of one of the modes is at its crest, while the field of the other mode is near its node. The required time for gaining the $\pi/2$ phase shift (for f_1 = 1.42 THz f_2 = 1.36 THz) matches the time delay t = 5 ps after the excitation for the field distribution in Fig. 4(c). This analysis supports the hypothesis that the field distribution captured in Fig. 4(c) corresponds to the field profile of a MD mode with a large projection of its magnetic moment on the z-axis.

3. Conclusion

The poly-crystalline TiO_2 microspheres investigated in this study exhibit the MD and ED Mie resonances in the range of 1.0-1.6 THz and 1.6-2.1 THz respectively. The MD resonance line-width for a single resonator is less than 40 GHz. The narrow line-width and the sub-wavelength size ($2r \approx \lambda/10$) make the TiO_2 microspheres excellent candidates for realizing the effective magnetic response for low-loss THz metamaterials. In comparison with SRR, the TiO_2 resonators can provide a narrower line-width at THz frequencies and eliminate the anisotropy and polarization dependence of the effective magnetic permeability μ [3,29].

The near-field scanning probe microscopy technique employed here enables us to probe individual high-permittivity TiO_2 resonators. The Mie resonance signatures, extracted using the THz time-domain spectroscopy method, appear as Fano resonances in the amplitude and phase spectra, whereas the electric field distribution near the microspheres helps identifying the resonance nature. The experimental observations allow us to correlate the variation of the MD resonance line-width with the resonator non-sphericity, which results in the splitting of the degenerate MD modes.